

- Sliding friction oldest problem in physics

Losses in US 6% gross national product US\$420×10⁹

Sliding friction is not just a nuisance

Without friction: no violin music, walk, drive a car, etc.

In some cases want to maximize the friction of tires of a car during braking.

- Sliding friction theoretical interest

Irreversibility

Adiabaticity

Self organization (critical)

Boundary lubrication:

dynamical phase transition in molecular thin lubrication layers

1- Introduction

The friction forces observed for macroscopic bodies are ultimately due to the electromagnetic forces between the electrons and nuclear particles.

An exact treatment of the interaction between two solids would consider the coupling between all the electrons and nuclei using microscopic equations of motion for these particles (quantum electrodynamics).

Microscopic Approach

- *two applications*

a)- an interesting applications of the Coulomb friction law $F = \mu L$ is in the calculations of the minimum speed of a vehicle from the length of its skid marks. The skid distance d can be obtained by the condition that the initial kinetic energy $Mv^2/2$ is entirely “dissipated” by the friction between the road and the wheels during the skid.

The friction force $F = \mu L$ where the load $L = Mg$. Thus μ can be taken as a constant during skid $Mv^2/2 = Fd$ or $Mv^2/2 = Mg\mu d$ so that $v = (2d\mu g)^{1/2}$.

Hence, if the Coulomb law is obeyed, the initial velocity is entirely determined by the coefficient of friction and the length of the skid marks. This simple result does not hold perfectly since the coefficient of friction μ tends to increase with increasing velocity. Nevertheless, properly applied measurements of the skid length provide a conservative estimate of the speed of the vehicle at the moment when the brakes were first applied and it has become a standard procedure for data of this kind to be obtained at the scene of a traffic accident.

b)- another application we show that friction explains why the pressure at the bottom of a container filled with sand is essentially independent of the filling height. This phenomenon is due to the fact that the forces are transmitted to the side walls such that the lower parts of the contents do not have to carry the weight of the part above. This is why the flow velocity in an hour-glass does not depend on the filling height. The constant pressure is in marked contrast to an incompressible liquid for which the pressure increases linearly with degree of filling.

To derive this result for a cylindrical container of radius R one starts by calculating the pressure increase $p(x)$ from the top ($x = 0$) to the bottom (see Fig. 1). Consider a horizontal slice of thickness Δx of weight $\pi R^2 \Delta x \rho g$ where ρ is the mass density which is assumed to be independent of x . The weight is partly compensated by the friction at the container walls. This friction is proportional to the normal force $L = 2\pi R \Delta x p(x)$. The total force on the slice Δx must equal zero so that

$$\pi R^2 [p(x + \Delta x) - p(x)] = \pi R^2 \Delta x \rho g - 2\pi R \Delta x \mu p(x)$$

$$\text{or } \frac{dp}{dx} = \rho g - \frac{2\pi \mu p}{R}$$

which can be integrated to give

$$p = \frac{\rho g R}{2\mu} \left(1 - e^{-2\mu x / R}\right)$$

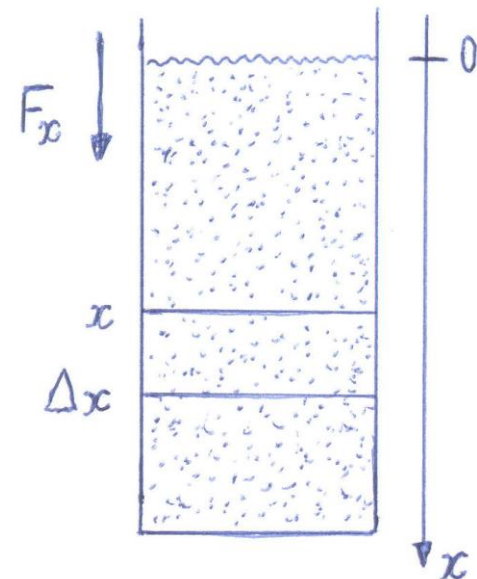


Fig. 1- A container filled with sand

Near the surface $x = 0$ the pressure increases linearly with x as in an incompressible fluid, but at a depth comparable to the radius of the container the pressure approaches a constant value. This model explains only the height dependence of the average pressure. In granular media pressure fluctuations are significant and experiments have shown that the forces are concentrated on an irregular network of contacts. Also, one expects thermally activated creep to occur, which results in a very slow increase of the pressure at the bottom of the container.

Modern Experimental Methods and Results

Practically all sliding friction devices have an interface where the friction force is generated, a finite sliding mass M , and some elastic properties usually represented by a spring k_s as in Fig. 2. The spring does not need to be an external spring but could represent the overall elastic properties of the sliding device. In most sliding friction experiments the free end of the spring moves with constant velocity v_s , but sometimes it varies with time. The force in the spring as a function of time is the basic quantity registered in most of these experiments. It is important to note that, due to inertia, during acceleration the spring force is not equal to the friction force acting on the block.

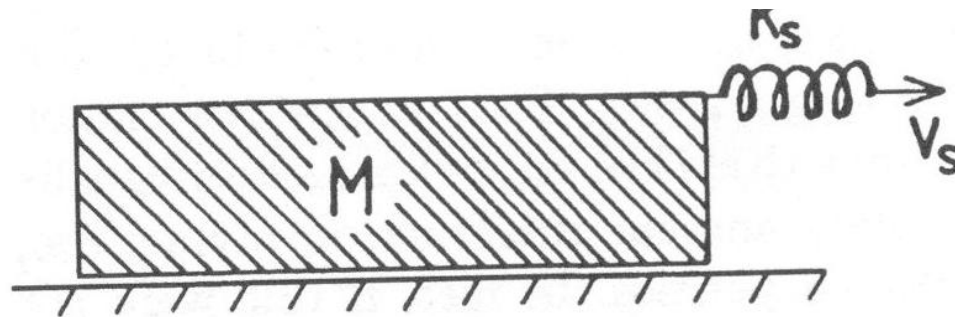


Fig. 2- A block with mass M sliding on a flat substrate. A spring constant (k_s) is connected to the block and the “free” end of the spring moves with the velocity v_s .

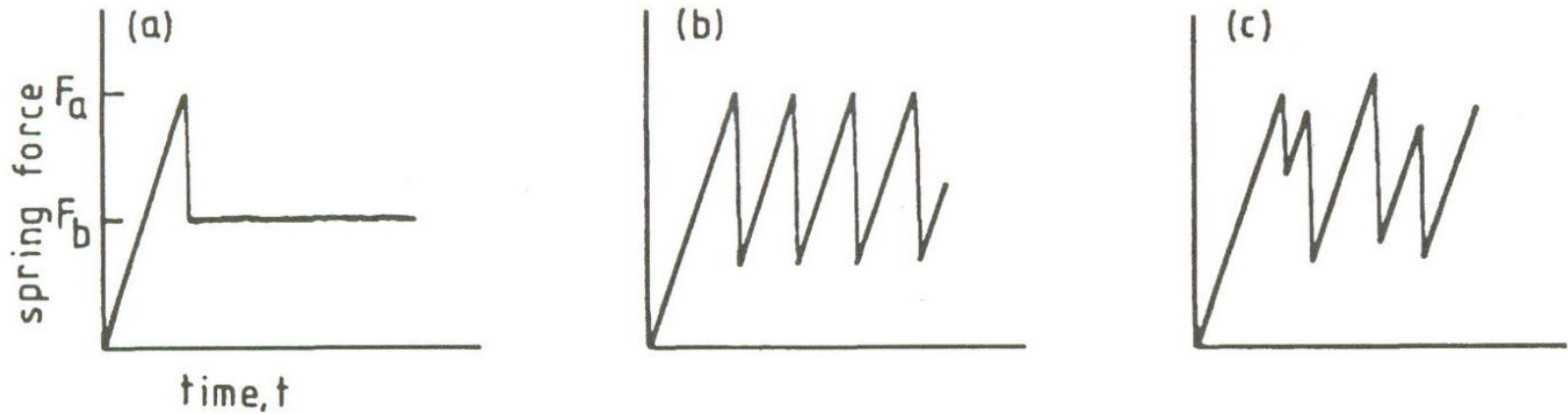


Fig. 3- Sliding dynamics of the block in Fig. 2 for three different cases: (a) steady sliding, (b) periodic stick-slip motion and (c) chaotic motion.

Figure 3 shows the spring force as a function of time for three different cases. Assuming that sliding starts with the spring at its natural length, the spring force initially increases linearly with time while the block is stationary. When the spring force reaches a critical value F_a , the so-called static friction force, the block starts to move. The motion is either of the steady type as in Fig. 3a, in which case the spring force equals the kinetic friction force F_b , or else stick-slip motion occurs, where the block alternates between stick and slip. One fundamental problem in sliding friction is to map out (and understand) the dynamical phase diagram, i.e., to determine the regions in the (k_s, v_s) plane where steady and stick-slip motion occur, and also the nature of the transitions between stick-slip and steady sliding, e.g., whether the transitions are continuous or discontinuous.

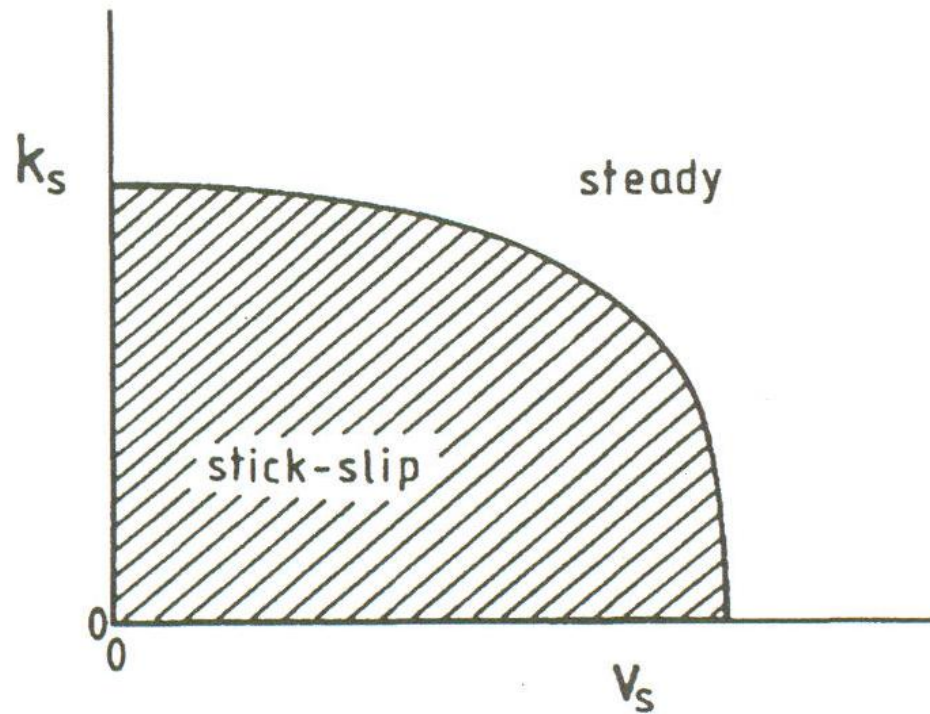


Fig. 4- General form of a kinetic phase diagram. The dashed region in the (k_s, v_s) plane denotes the values of k_s and v_s for which the motion is of the stick-slip nature.

It is an experimental observation that stick-slip always disappears if the spring k_s is stiff enough, or if the sliding velocity v_s is high enough; see Fig. 4. Hence, the kinetic friction force F_b can always be measured by making the spring k_s so stiff that the motion is steady. Note also that during stick-slip motion the oscillations in the spring force are not always periodic as in Fig. 3b, but sometimes behave chaotically as in Fig. 3c. Non-periodic stick-slip motion may result from various sources, e.g., from the intrinsic nonlinear properties of the equations of motion, or simply from surface inhomogeneities, e.g., randomly distributed areas of “dirt”, with an average spacing on the order of, or longer than, the linear size L of the block. If the average separation between the surface inhomogeneities were much smaller than L , the fluctuations in the friction force would be negligible. From random-walk arguments, the fluctuation δF in the friction force F due to surface inhomogeneities with the concentration n , is $\delta F \propto (nA)^{-1/2}$ where A is the surface area.

2- Surface Forces Apparatus

Sliding friction studies have been performed on two different classes of adsorption systems as illustrated in Fig. 5. The first class consists of “inert” molecules, e.g., hydrocarbon fluids or silicon oils. In these cases the adsorbate-substrate interaction potential is relatively weak and, more importantly, the lateral corrugation of the adsorbate-substrate interaction potential is very small.

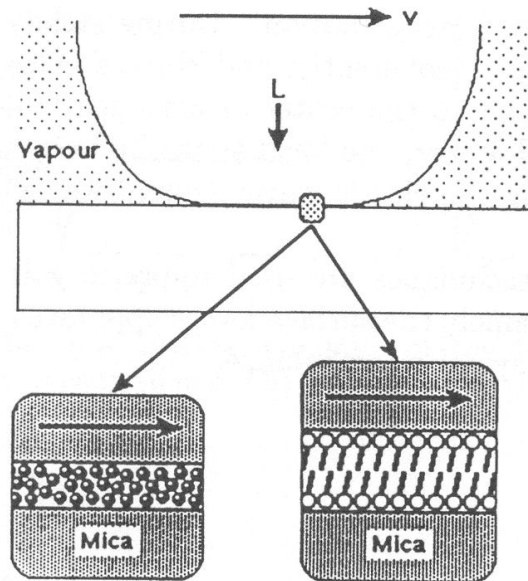


Fig. 5- Schematic representation of the contact region of two lubricated mica surfaces in a surface force apparatus experiment.

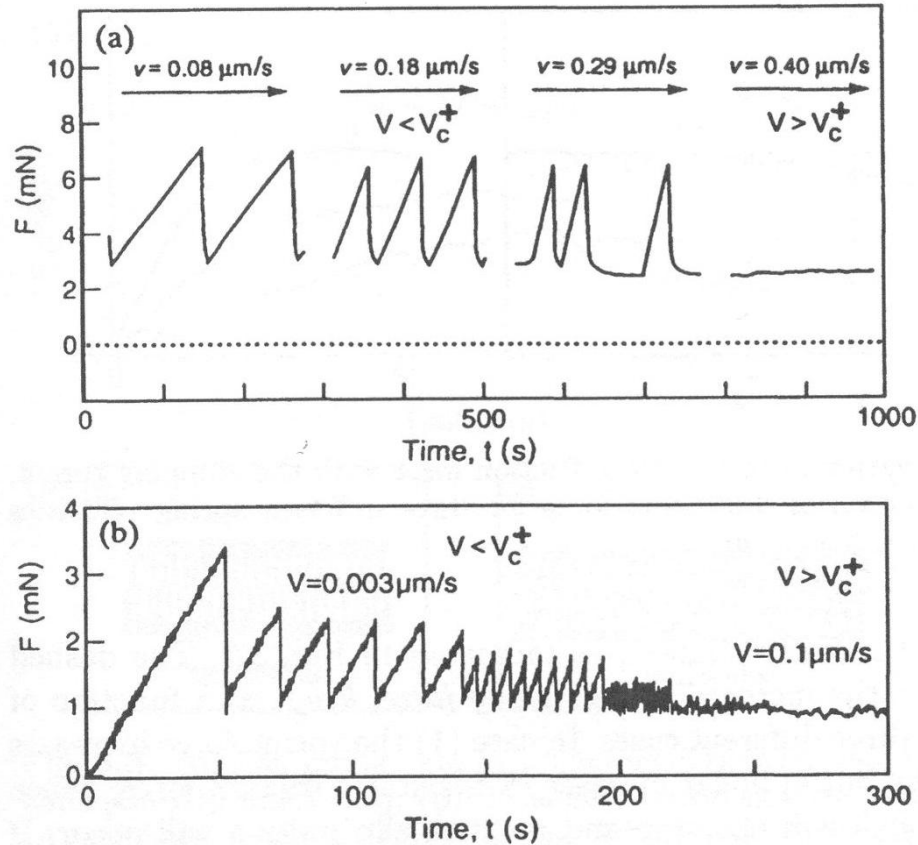


Fig. 6- The spring force F as a function of time t for (a) a hydrocarbon liquid (hexadecane) and (b) for mica surfaces coated with end-grafted chain molecules (DMPE). When the spring velocity increases beyond v_c^+ the sliding motion becomes steady, where $v_c^+ \approx 0.3 \mu\text{m/s}$ in case (a) and $v_c^+ \approx 0.1 \mu\text{m/s}$ in case (b).

As an example, Fig. 6a shows the spring force as a function of time, at several spring velocities v_s , for a 12 Å thick hexadecane ($C_{16}H_{34}$) film. Note that for $v_s < v_c^+$, where $v_c^+ \approx 0.3 \mu\text{m/s}$, stick-slip oscillations occur while an abrupt transition to steady sliding occurs when v_s is increased above v_c^+ (note: v_c and v_c^+ denote the spring velocities at the transition between stick-slip and steady sliding, when the spring velocity is reduced from the steady sliding region, and increased from the stick-slip region, respectively). The second class of systems includes grafted chain molecules, e.g., fatty acids on mica or on metal oxides. In these cases the corrugation of the adsorbate-substrate interaction potential is much stronger, and usually no fluidization of the adsorbate layers occurs; the sliding now occurs at the plane where the grafted chains from the two surfaces meet.

- Large Corrugation

The decrease in the amplitude of the stick-slip spikes in Fig. 6b with increasing v_s can be understood as follows. Let us consider the molecules at the interface during a stick time period. The minimum free energy configuration may involve some interdiffusion of the hydrocarbon chains from the two monolayer films, or some other molecular rearrangement process. However, a large (on the scale of the thermal energy $k_B T$) free energy barrier may separate the interdiffused state from the state where no interdiffusion has occurred and a long time τ may be necessary in order to reach the thermal equilibrium state. For low spring velocity v_s the system spends a long time in the pinned state and nearly complete interdiffusion may occur, leading to a “large” force necessary to break the pinning. Thus “high” stick-slip spikes occur at “low” spring velocity. As the spring velocity increases, the system will spend less time in the pinned state before the critical stress (necessary for initiating sliding) has been reached, resulting in less interdiffusion and a smaller static friction force. Thus the amplitude of the stick-slip spikes is expected to decrease with increasing spring velocity.

- Small Corrugation

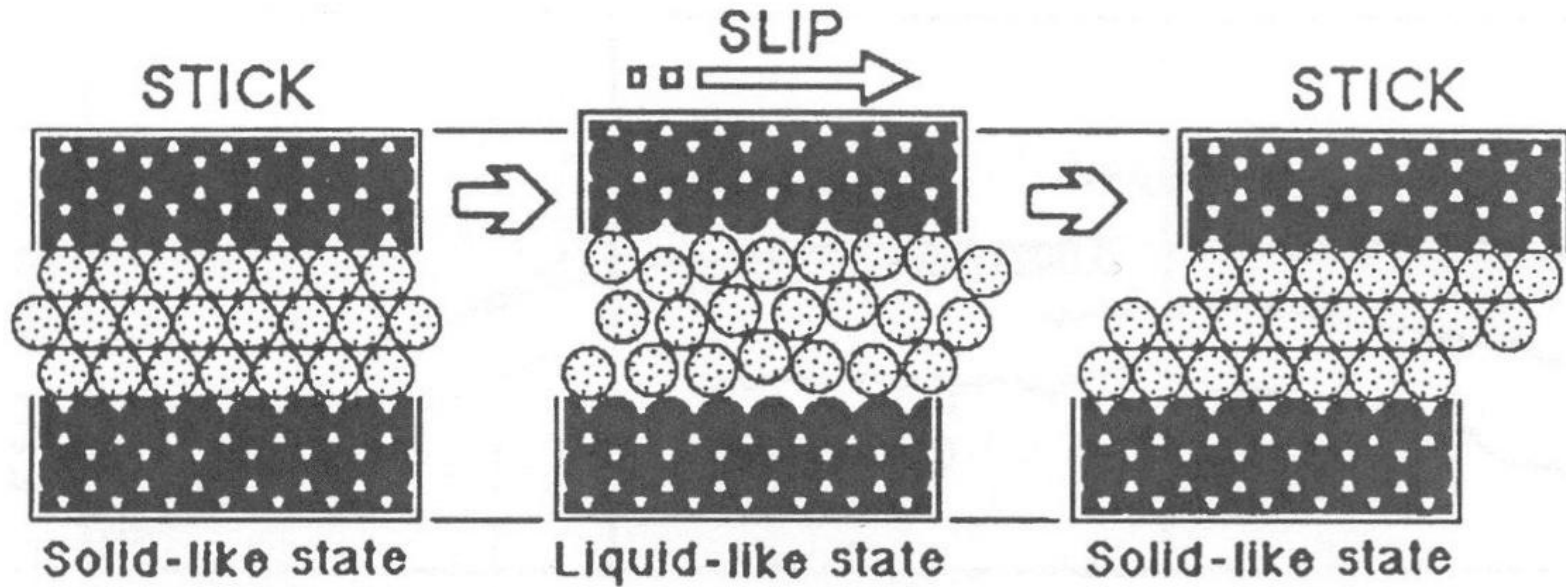


Fig. 7- During stick-slip motion the lubrication film alternates between a frozen solid state and a liquid or fluidized state.

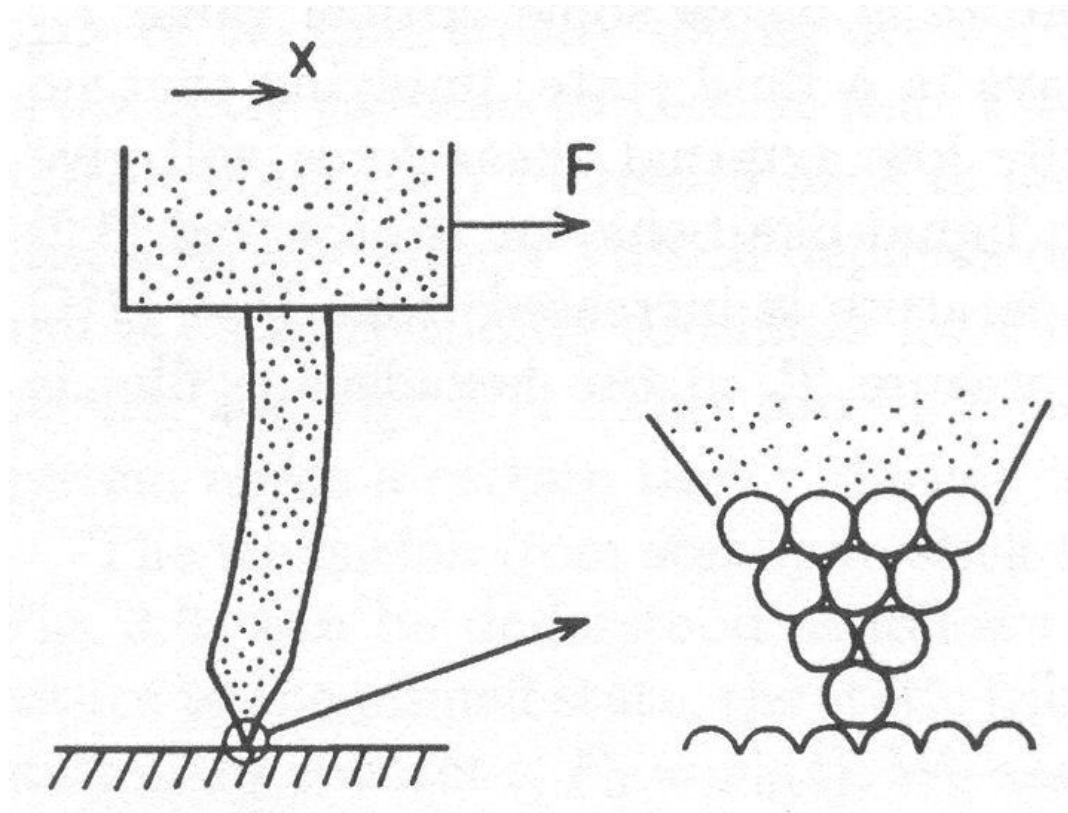


Fig. 8- Schematic diagram shows a sharp tip made from, e.g., tungsten or diamond, sliding over a substrate.

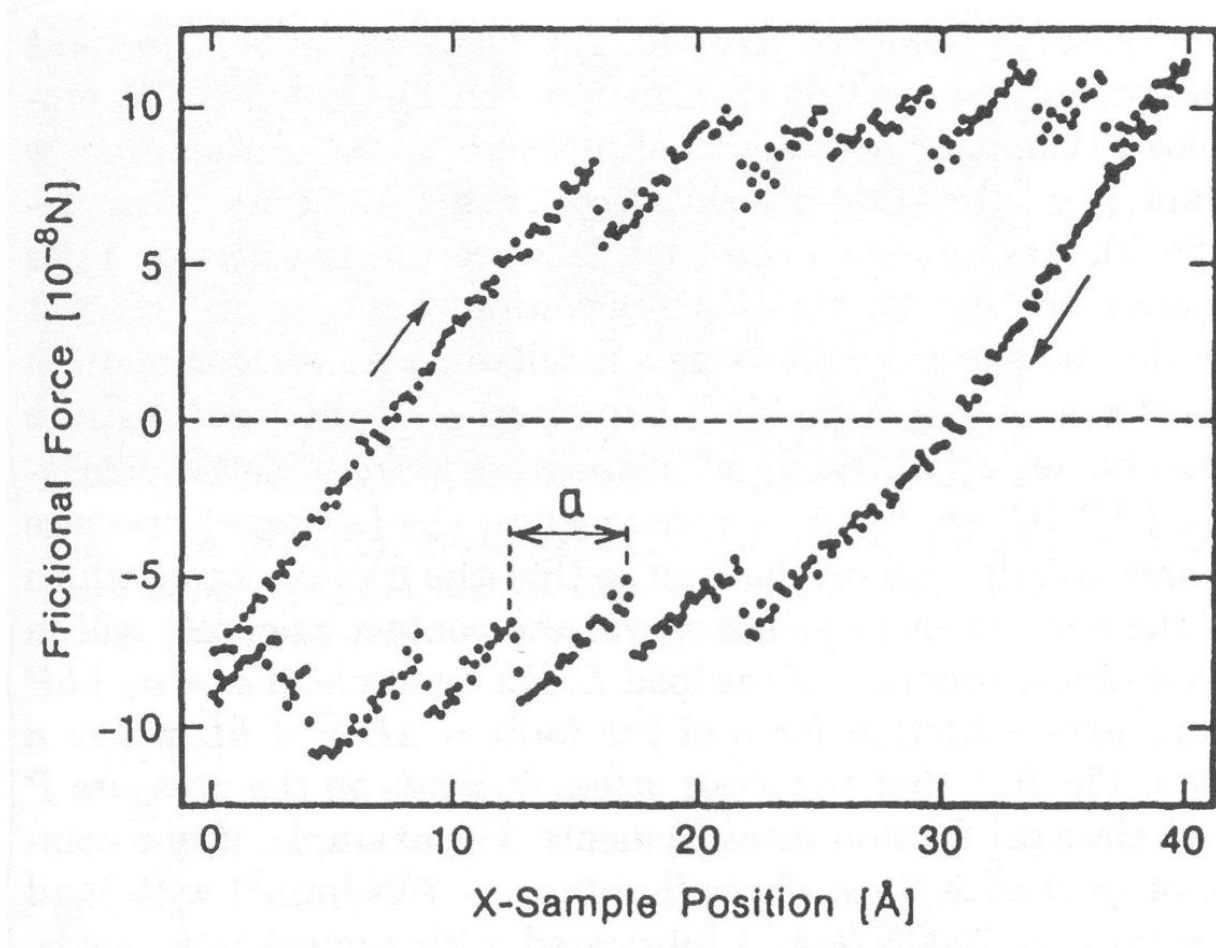


Fig. 9- The sliding force in the z-direction as a function of sample position as a tungsten tip is scanned back and forth on a mica surface. The substrate lattice constant $a \approx 5 \text{ \AA}$.

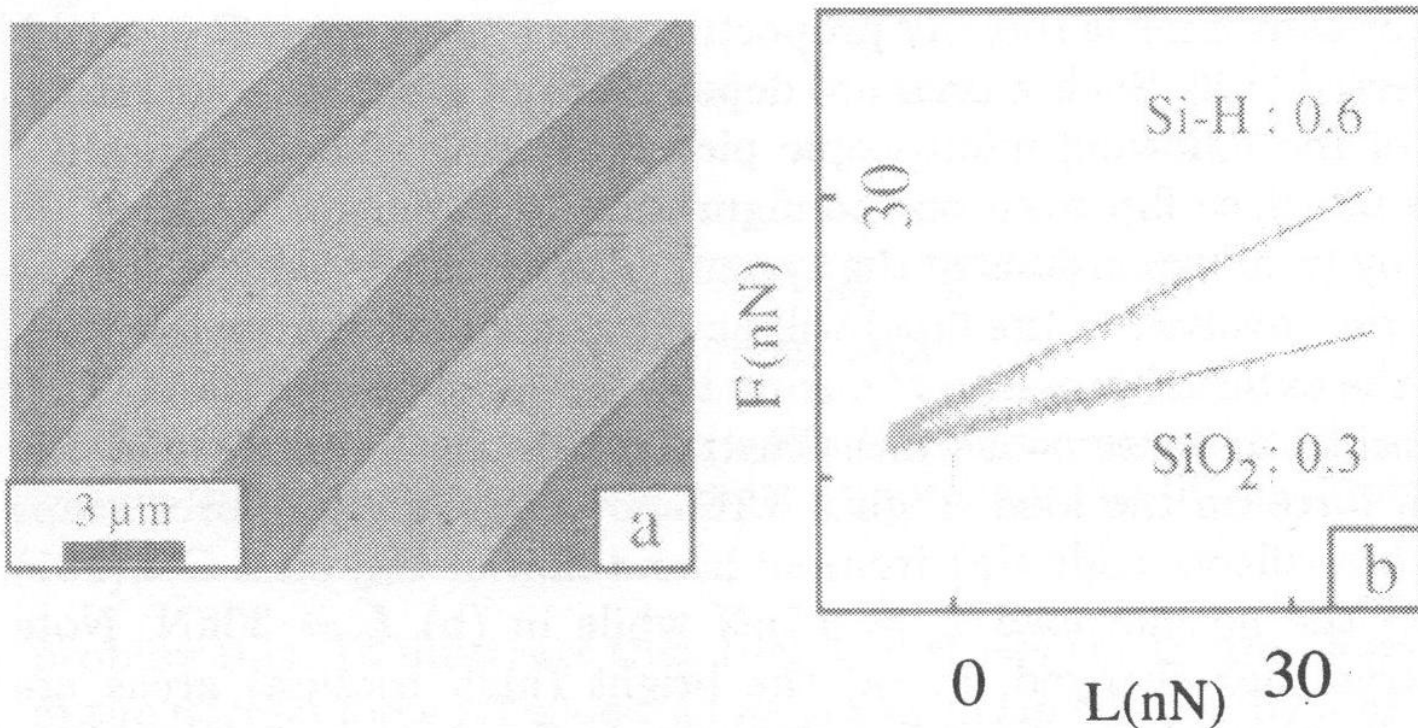


Fig. 10- (a) Friction force map of Si/SiO₂ grid etched in 1:100 HF/H₂O. The bright area corresponds to high friction and is observed on the Si-H whereas the friction on SiO₂ is lower by a factor of two. (b) The relation between the friction force F and the load L on the SiO₂ and Si-H areas in (a). Note the linear dependency $F = \mu L$ where $\mu = 0.6$ on Si-H and $\mu = 0.3$ on SiO₂.

3- Area of Real Contact

Elastic and Plastic Deformations

The friction force equals the shear stress integrated over the area ΔA of real contact. Because of surface roughness, the area of real contact is usually much smaller than the apparent area of contact. Here we discuss the physical processes which determine the area of real contact and present some experimental methods which have been used to estimate ΔA . In most practical applications, the diameter of the contact areas (junctions) is on the order of ~ 10 μm . However, the present drive towards microsystems, e.g., micromotors, has generated a great interest in the nature of nanoscale junctions. The physical processes which determine the formation and behavior of nanoscale junctions are quite different from those of microscale junctions. We consider first microscale junctions and then nanoscale junctions.

3.a- Microscale Junctions

- *Elastic Deformations*

In the surface force apparatus two crossed glass cylinders covered with atomically smooth mica sheets are pressed together to form a small circular contact area with a radius r_0 which depends on the load F . In these measurements the force F is so small that only elastic deformation occurs and the radius r_0 as a function of the load F can be calculated using the theory of elasticity. This problem was first solved by H. Hertz. A simple derivation of the size of the contact area formed when two homogeneous and isotropic elastic bodies of arbitrary shape are pressed together can be found in the book by Landau and Lifshitz. Here we only quote the results for two spheres with radius R and R' . The contact area $\Delta A = \pi r_0^2$ is a circular region with radius

$$r_0 = \left(\frac{RR'}{R + R'} \right)^{1/3} (\kappa F)^{1/3}, \quad \text{where} \quad \kappa = \frac{3}{4} \left(\frac{1 - \nu^2}{E} + \frac{1 - \nu'^2}{E'} \right), \quad (1)$$

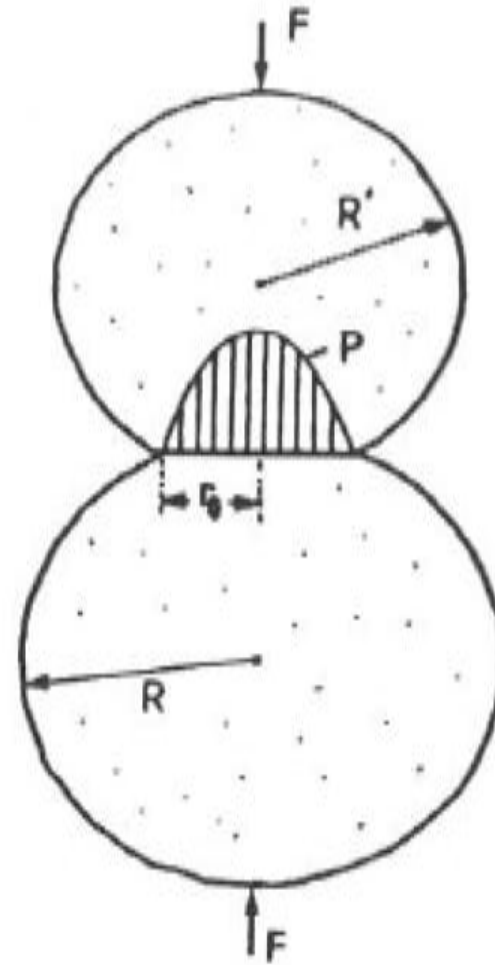


Figure 11- Elastic deformation and pressure distribution in the contact area between two elastic solids.

with E and ν the elastic modulus and Poisson number, respectively. The distance h by which the two spheres approach each other (i.e., h is the difference between $R + R'$ and the distance between the centers of mass of the two bodies after contact) is given by

$$h = \left(\frac{R + R'}{RR'} \right)^{1/3} (\kappa F)^{2/3} \quad (2)$$

The pressure distribution in the contact area has the form (Fig. 11)

$$P(x, y) = P_0 \frac{3}{2} \left[1 - \left(\frac{r}{r_0} \right)^2 \right]^{1/2} \quad (3)$$

where $P_0 = F/\pi r_0^2$ is the average pressure and $r = (x^2 + y^2)^{1/2}$ is the distance from the center of the circular contact area. Note that the pressure goes continuously to zero at the periphery of the contact area, i.e., for $r = r_0$ and that the pressure at the center $r = 0$ is a factor $3/2$ higher than the average pressure P_0 .

- Area of Real Contact: Elastic and Plastic Deformations

Let us approximate a surface as consisting of N elastic spherical caps with the same radius R but with different heights, which are pressed against a rigid flat plane, see Fig. 12. Let $N\Phi(z)dz$ be the number of spheres with heights between z and $z + dz$, i.e., $\Phi(z)$ is the height probability distribution function. All asperities of height greater than d will make contact and will be compressed a distance $h = z - d$. Assuming elastic deformations, using equations (1) and (2), the asperity contact area equals $\pi r_0^2 = \pi R h = \pi R(z - d)$ and the asperity load equals $R^{1/2} \cdot h^{3/2} / \kappa$. Thus the total number of contacts is

$$\Delta N = \int_d^{\infty} dz N \Phi(z)$$

the area of real contact $\Delta N = \int_d^{\infty} dz N \Phi(z) \pi R (z - d)$

and the total load $L = \int_d^{\infty} dz N \Phi(z) R^{1/2} (z - d)^{3/2} / \kappa$

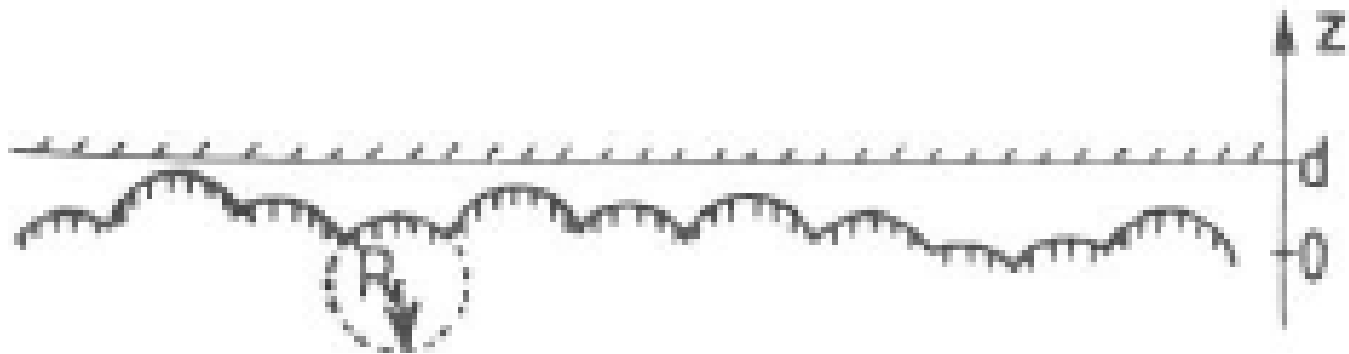


Fig. 12- Contact between a rough surface and a rigid plane. All asperities of height z greater than the separation d make contact.

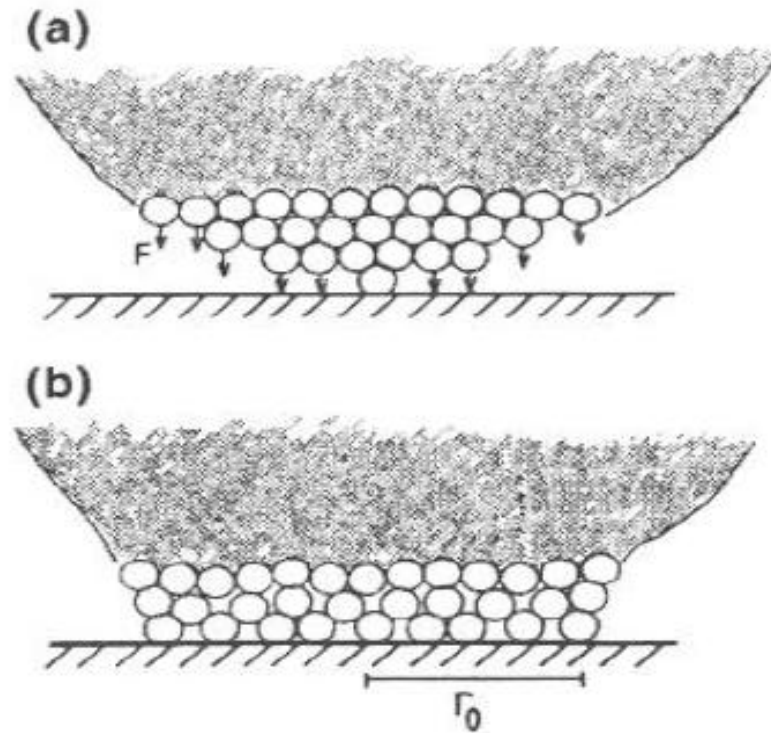


Fig. 13- (a) A rigid tip in atomic contact with a (rigid) substrate. The vertical arrows indicate the force acting on the tip atoms from the substrate. (b) For a real tip with finite elastic (and plastic) properties the tip atoms in the vicinity of the substrate will move into direct contact with the substrate over a region with radius r_0 .

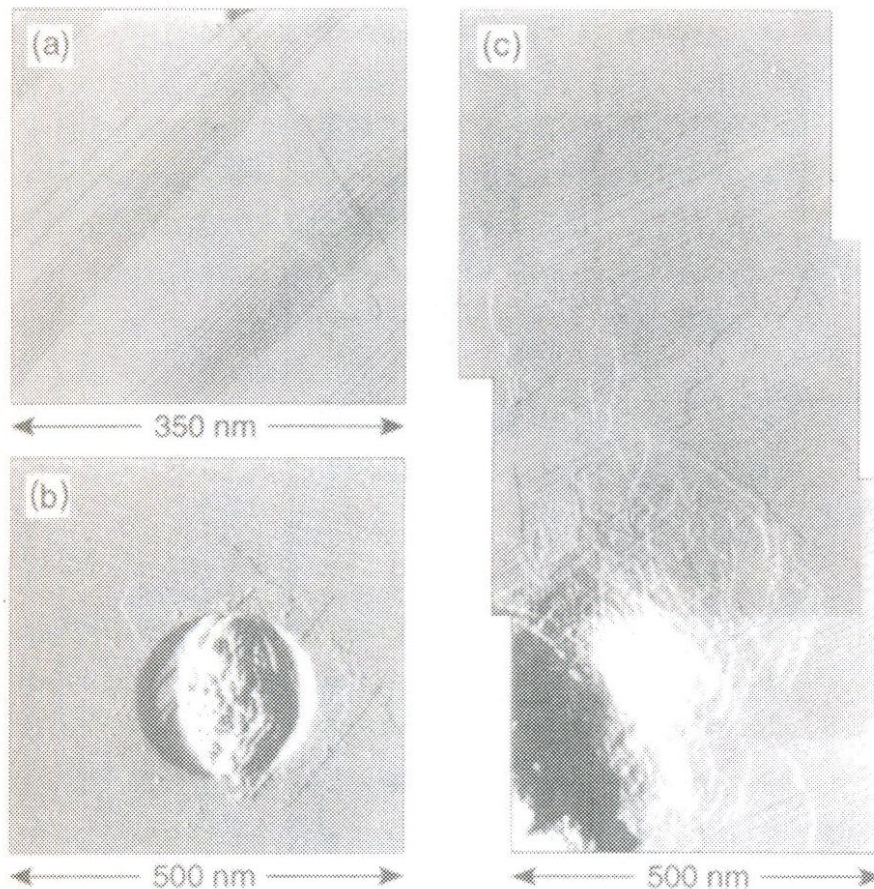


Fig. 14- Contact footprint recorded after indentation of an Ir tip into a Pt(111) substrate. Indentation depth is approximately 1 nm, 2nm and 5nm for (a,b,c) respectively. The pattern of quasi-parallel rows of monatomic steps is intrinsic to the substrate and reflects the local miscut of the surface. A hillock several nanometers high is always produced at the point where contact was made. In addition, monatomic steps with more or less random orientation are observed. These steps originate from vertical displacements of the sample surface that are produced by dislocations within the bulk with Burgers vectors perpendicular to the surface.

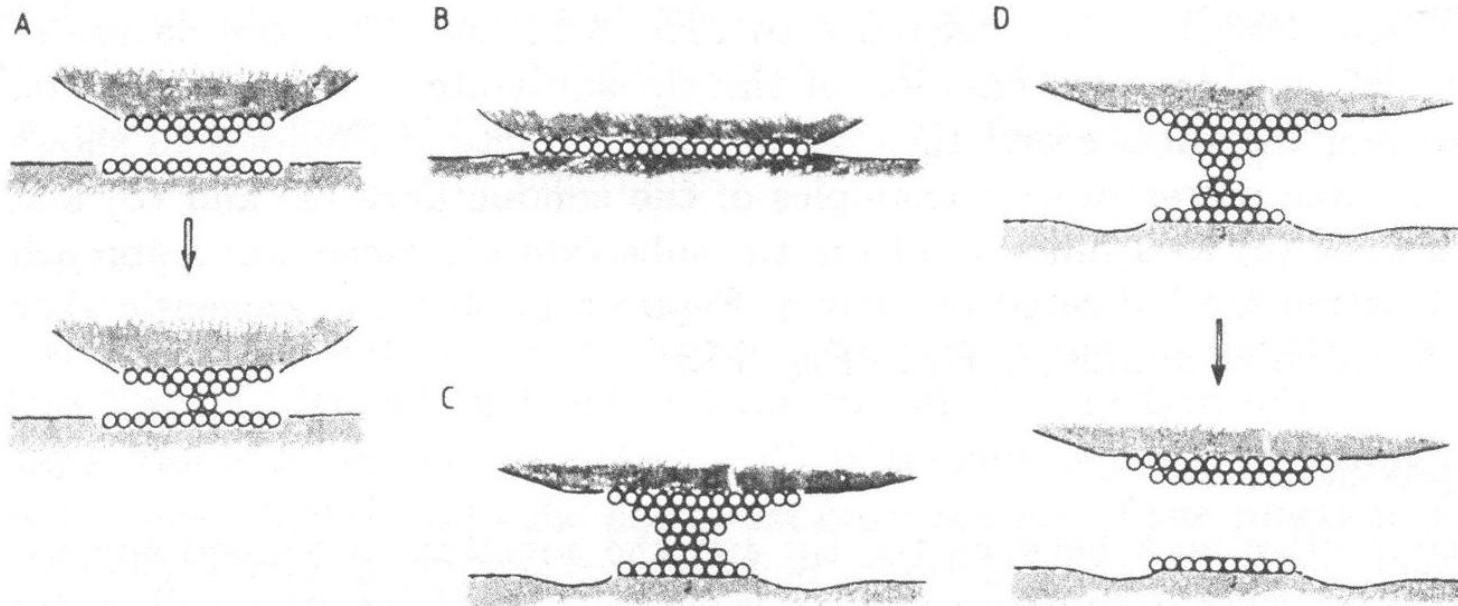


Fig. 15- Artistic view of the deformation on applied force as a function of the tip-sample displacement.

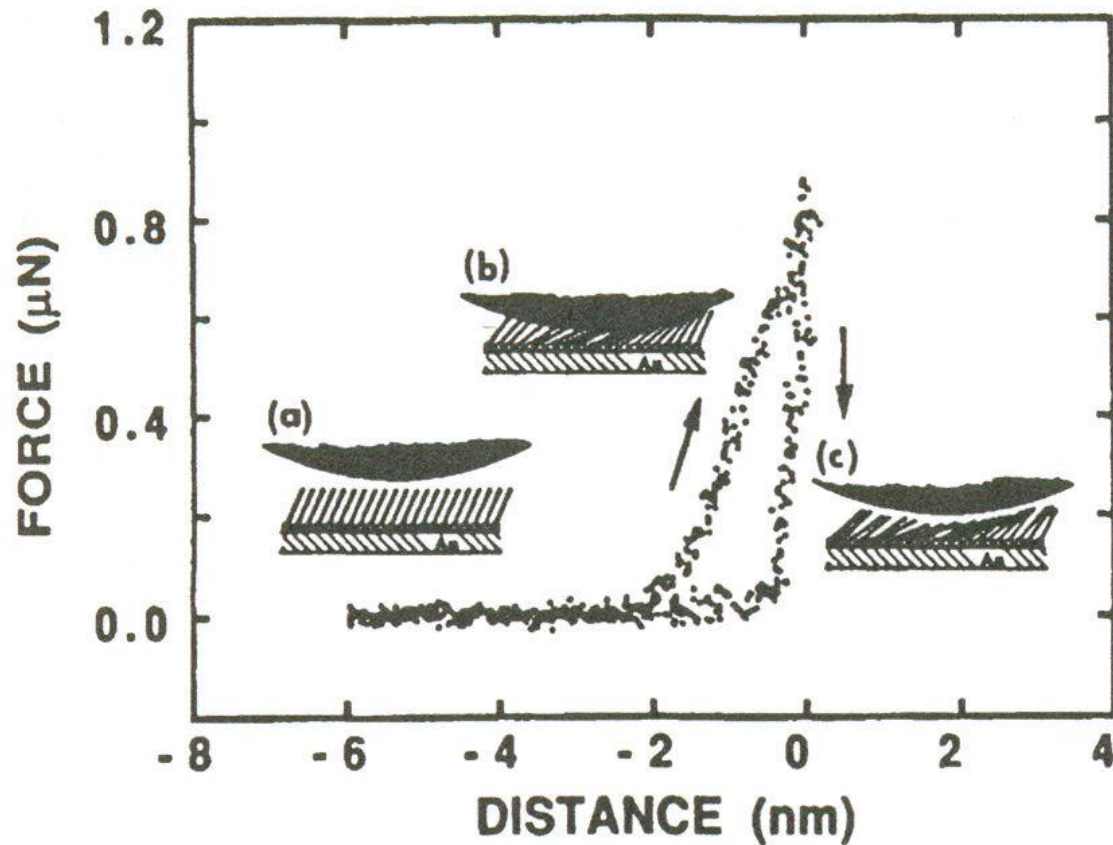


Fig. 16- The tip force as a function of the tip-sample separation. The rate of perpendicular displacement is 50 \AA/s . The zero separation is arbitrary assigned to the point at which the motion changes direction.

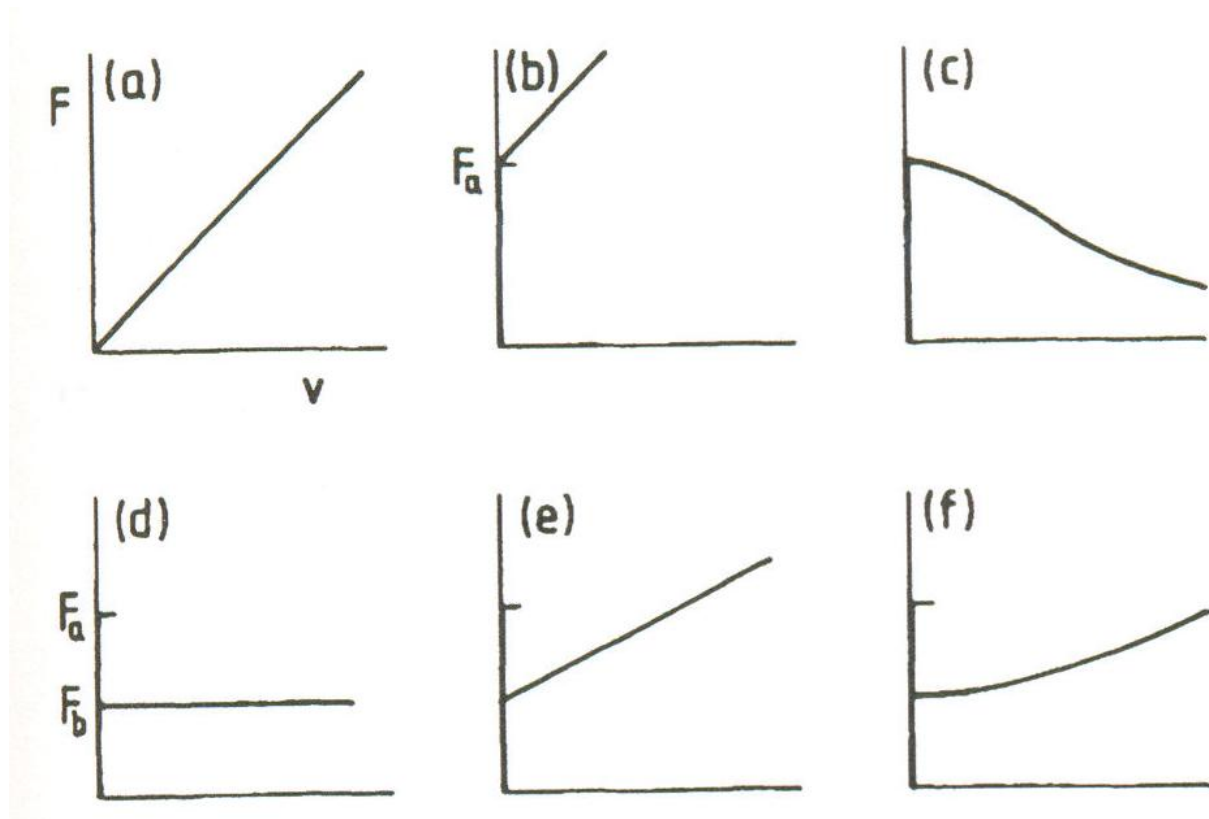


Fig. 17- The friction "law" is given by (a) $F_0 = F_a v/v_0$ while in cases (b – f), $F_0 \leq F_a$ if $v \geq 0$, (b) $F_0 = F_a(1 + v/v_0)$, (c) $F_0 = F_a/[1 + (v/v_0)^2]$, (d) $F_0 = F_b$ ($F_b < F_a$), (e) $F_0 = F_b(1 + v/v_0)$ and (f) $F_0 = F_b[(1 + (v/v_0)^2)^{1/2}]$.

- Sliding Dynamics Resulting from Simple Friction Laws

Consider a block of mass M on a substrate and assume that a spring with force constant k_s is connected to the block as indicated in Fig. 2. Assume that the block is rigid and that the free end of the spring moves with the velocity v_s . In this section we discuss the nature of the motion of the block, under the assumption that the friction force, $-F_0(t)$, only depends on the instantaneously velocity $\dot{x}(t)$ of the block. In particular, we consider the friction “laws” (a - f) indicated in Fig. 17. As will be shown below, using friction laws which only depend on the instantaneously velocity $\dot{x}(t)$ is, in general, not a good approximation.

Let $x(t)$ be the position coordinate of the block at time t and assume that at $t = 0$ the block is stationary relative to the substrate [$x(0) = 0$ and $(0) = 0$] and that the spring force vanishes. Now, for “low” spring velocities v_s the solid block is either in a pinned state relative to the substrate (i.e., $= 0$) in which case the friction force is $F_0 \leq F_a$ (in Fig. 17a the static friction force vanishes), or else in a sliding state where the friction force equals $F_0(v)$ given by Fig. 17. The equation of motion for the block has the form

$$M\ddot{x} = k_s (v_s t - x) - F_0 \quad (1)$$

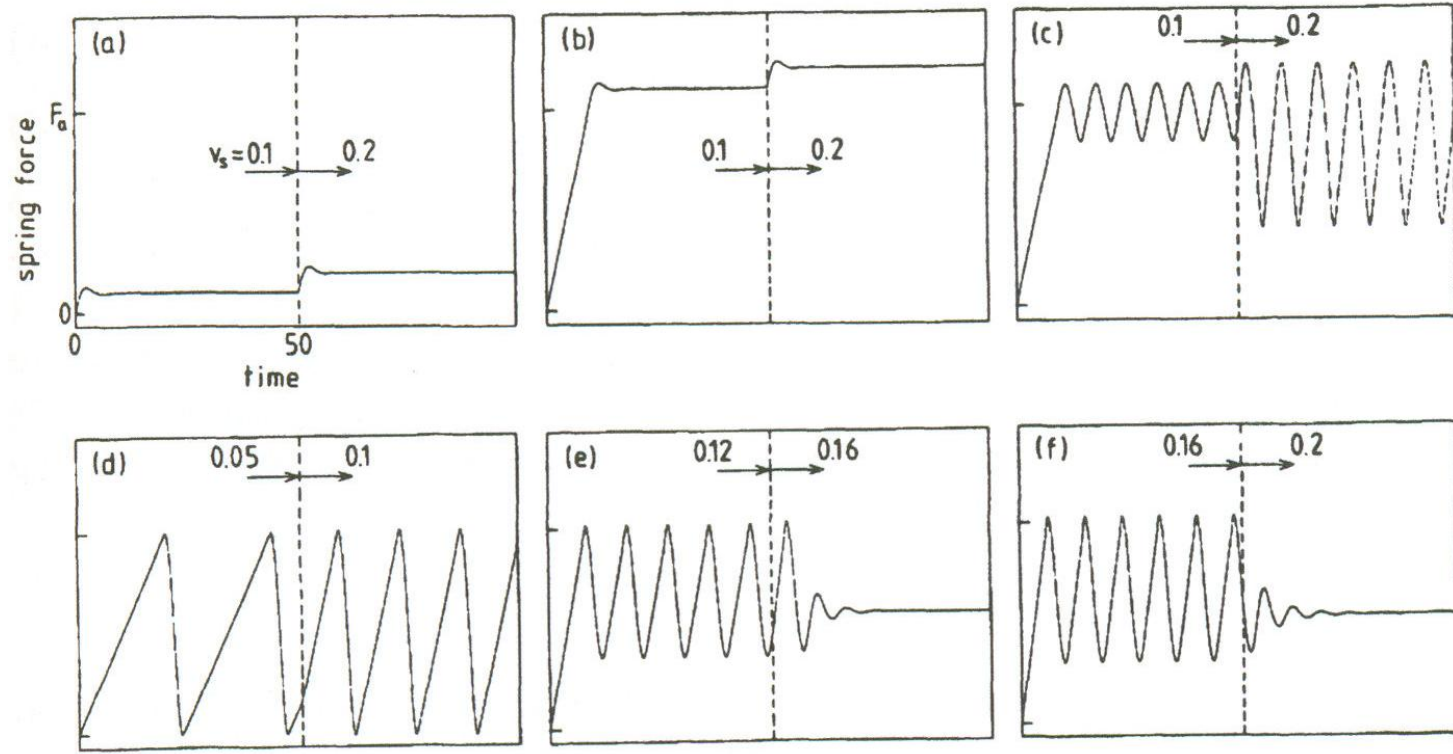


Fig. 18- The spring force F_s as a function of time for the friction laws (a – f). In all cases, $F_b = F_a/2$ and $v_0 = 1$ while in cases (a – c), $v_s = 0.1$ for $t < 50$ and 0.2 for $t > 50$ and in case (d), $v_s = 0.05$ for $t < 50$ and 0.1 for $t > 50$, and in case (e), $v_s = 0.12$ for $t < 50$ and 0.16 for $t > 50$, and in case (f), $v_s = 0.16$ for $t < 50$ and 0.2 for $t > 50$.

If we measure time units of $(M/k_s)^{1/2}$, distance in units of F_a/k_s , velocity in units of $F_a(Mk_s)^{-1/2}$ and the friction force F_0 in units of F_a then the previous equation (eq. 1) takes the form

$$\ddot{x} = v_s t - x - F_0$$

In Fig. 18 we show the spring force $F_s = v_s t - x(t)$ as a function of time. The different curves have been calculated using the friction “laws” (a–f) of Fig. 17 and in all cases the spring velocity increases abruptly at $t = 50$, as indicated in Fig. 18. In cases (a) and (b) smooth sliding occurs for all values of v_s and k_s . In cases (c) and (d) stick-slip motion occurs for all parameter values. Finally, in cases (e) and (f) stick-slip motion occurs when v_s is below some critical value v_c^+ which depends on k_s , while smooth sliding occurs when $v_s > v_c^+$.

Let us analyze cases (d) and (f) in more detail. The result shown in Fig. 18d can be understood as follows: Initially, as time increases the spring will extend, but the solid block will not move until the force in the spring reaches F_a . At this point the two surfaces can start to slide relative to each other. During sliding the friction force is $F_b < F_a$ and since the spring force is F_a at the onset of sliding block will initiate accelerate to the right. Note that owing to the inertia to the inertia of the block, the velocity \dot{x} is initially lower than v_s and the spring will continue to extend for a while before finally $\dot{x} > v_s$. The maximum spring force will therefore not occur exactly at the onset of sliding but slightly later, where the spring force is greater than F_a . In Fig. 18d this inertia effect is very small (this is typically the case in sliding friction experiments) and the maximum spring force is nearly equal to F_a . When the sliding velocity $\dot{x} > v_s$ the spring force decreases, but the analysis presented below shows that the sliding motion does not stop when the spring force equals F_b but continues until it reaches $\approx 2F_b - F_a$ where the motion stops and the whole cycle repeats itself. This model is simple enough that one can analytical evaluate the amplitude ΔF of the oscillations in the spring force which occur during sliding, as well as the stick and slip periods.

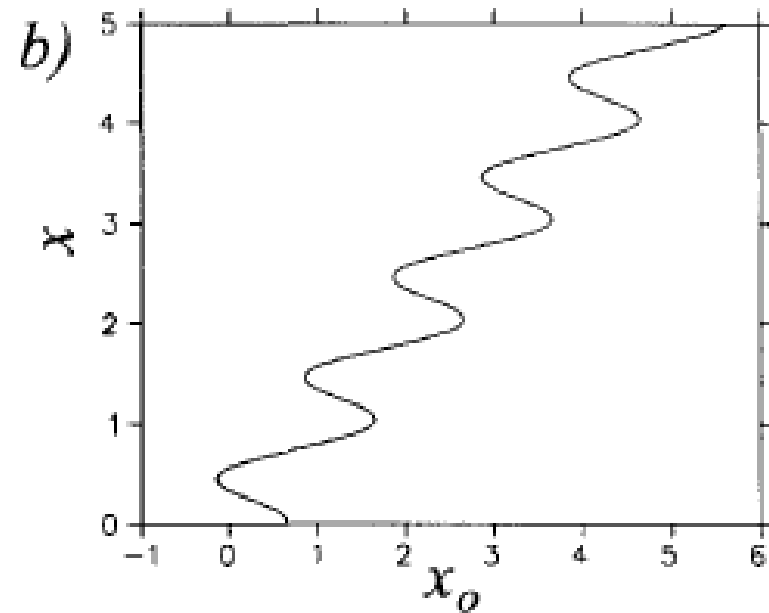
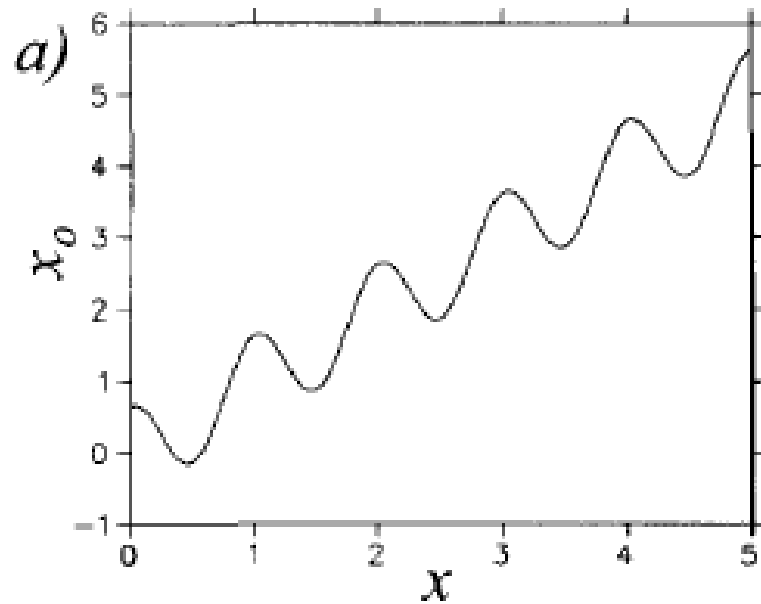


Figure 19- The mapping $\vec{r}(\vec{r}_0)$ contains folds for $c < c_{\text{crit}}$

One-dimensional Tomlinson model

We consider the tip of a FFM in a one-dimensional periodic potential, which represents the interaction with an atomically flat surface. We will concentrate on the quasistatic limit, of vanishing relative velocity of the two bodies. The total energy is given by the sum of the potential at the position x of the tip on the surface and the elastic energy which is stored in the cantilever.

$$E_{tot} = V(x) + \frac{c}{2} (x - x_0)^2 \quad (1)$$

where c is the spring constant of the cantilever and x_0 is the position of the support of the microscope. In our case, it is the position of the tip on the atomic surface, which is the system variable, whereas x_0 is the control variable. In a quasi-static process, the system variables arrange themselves always in a stable equilibrium. Mathematically, this condition means that the derivative of the energy with respect to the system variable is zero and that the second derivative is positive:

$$\frac{dE}{dx} = \frac{dV}{dx} + c(x - x_0) = 0 \quad (2)$$

$$\frac{d^2E}{dx^2} > 0 \quad (3)$$

The equilibrium condition can be rewritten in the form

$$x_0 = \frac{1}{c} \frac{dV}{dx} + x \quad (4)$$

This equation consists of a linear and a periodic term. Therefore, for small values of the spring constant c it is not invertible (see Fig. 19). We define the critical spring constant c_{crit} to be the smallest value of c above which the mapping (eq. 4) is invertible.

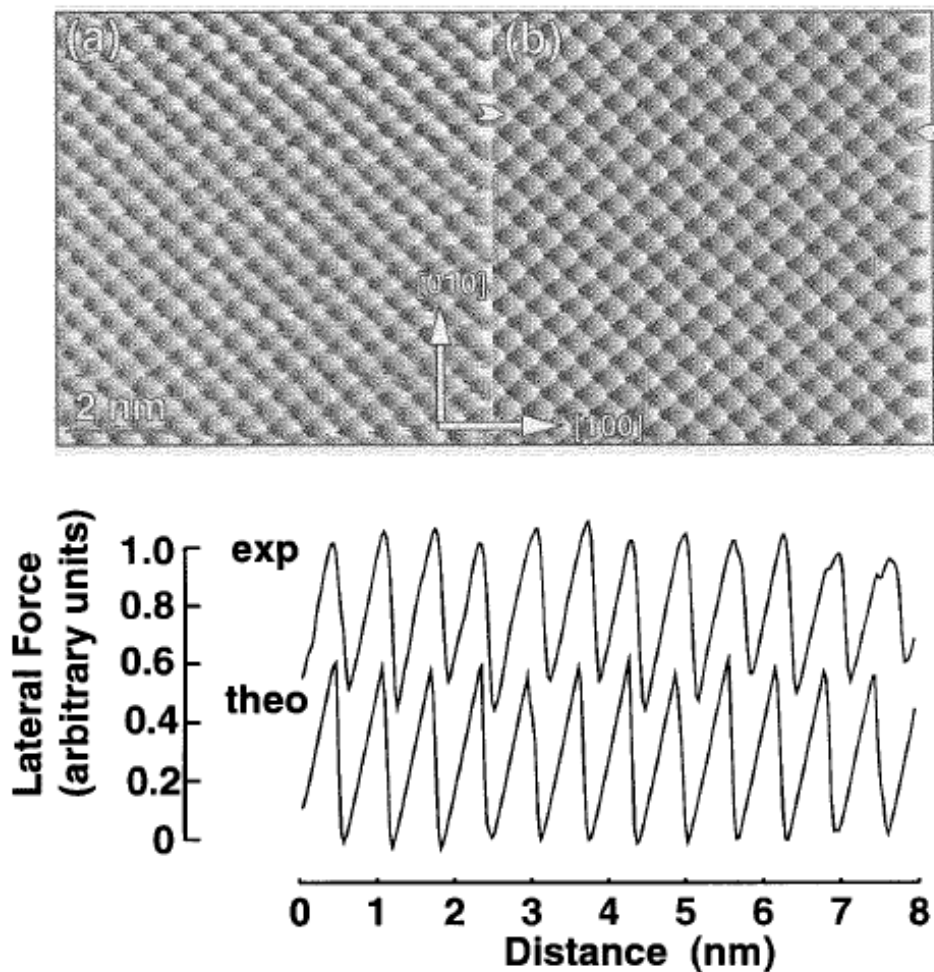


Figure 20- (a) Measured lateral force map. The experiment was performed in UHV with a Si-tip. As shown in the profiles, the typical atomic-scale stick-slip is revealed in both images. The slope of the lateral force curve during the sticking part is about 7 N/m. Taking into account the torsional spring constant of the cantilever of 32 N/m, one can estimate the lateral contact stiffness to be about 10 N/m. Thus, the softest spring is due to the sample/tip elasticity.

Comparison of atomic-scale stick slip with the Tomlinson plucking mechanism

The first friction force image on a nanometer scale has been obtained by Mate et al. They observed that friction force scans show a sawtooth-like behavior with the periodicity of the crystalline substrate. From the area that is enclosed by the friction force loop, one can directly calculate the energy that is dissipated.